

Preresonance Raman Single-Crystal Measurements of Electronic Transition Moment Orientations in *N*-Acetylglycinamide

Vasil Pajcini and Sanford A. Asher*

Contribution from the Department of Chemistry, University of Pittsburgh, Pittsburgh, Pennsylvania 15260

Received February 10, 1999. Revised Manuscript Received September 17, 1999

Abstract: We have examined electronic coupling between the two amide electronic transitions in a dipeptide and have found strong excitonic interactions in a case where the amide planes are almost perpendicular. We compared the absorption and resonance Raman spectra of *N*-methylacetamide (NMA) and acetamide (AM) to that of the dipeptide *N*-acetylglycinamide (NAGA), which is composed of linked primary and secondary amides. We measured the transition moment magnitudes of each of these species and also determined the orientation of the preresonance Raman tensor of NAGA in a single crystal. From these single-crystal tensor values, we calculated the NAGA diagonal Raman tensor orientations and compared them to those expected for unperturbed primary and secondary amides oriented as in the NAGA crystal. Because the primary and secondary amide III vibrations are vibrationally uncoupled and nonoverlapping, we can use their intensities to determine the contributions to their resonance enhancement from the coupled NAGA electronic transitions. The Raman tensor major axes of the primary and secondary amide III and amide I vibrations do not lie in their corresponding amide planes, indicating excitonically coupled states which mix the primary and secondary amide transitions. These results are relevant to the understanding of amide coupling in peptides and proteins; the NAGA crystal conformation is similar to that of a type I β -turn in peptides and proteins, with the amide planes nearly perpendicular to each other (dihedral angle 85°).

Introduction

The electronic properties of macromolecules can either result from the uncoupled or coupled electronic responses of individual molecular fragments.^{1,2} This coupling could derive from a delocalization of the electronic transitions between linked chromophores in a through-bond manner, similar to that which occurs for the conjugated π network of a polyene, or the interaction may occur through space, through excitonic interactions between the transition dipoles of the linked fragments with similar electronic transition energies.

In proteins and peptides, the conventional understanding of the backbone electronic excited states and transitions is that the backbone linked amide fragments interact only through excitonic interactions without any through-bond mixing of their excited states.^{3,4} In α -helical peptides, for example, these through-space excitonic interactions are proposed to result in two electronic transitions oriented parallel and perpendicular to the helix axis.^{3,5,6} However, this established view of peptide transitions completely neglects the possibility of through-bond interactions of the excited states which could lead to delocalization of the excited states of the amide fragments.

We recently examined the electronic transitions and excited states of the simplest dipeptide, glycyl-glycine (Gly-Gly), and discovered intimate electronic coupling between the amide and carboxylate groups.⁷ This coupling results in a new charge-transfer transition at ~ 200 nm, which involves electron transfer from a nonbonding carboxylate orbital to the π^* orbital of the amide group.⁷ We also measured the direction of this charge-transfer transition moment as well as the orientations of the amide and carboxylate NV_1 ($\pi \rightarrow \pi^*$) transition moments in a hydrated crystal of Gly-Gly.⁸ The charge-transfer transition moment was found to be oriented along the axis connecting the carboxylate and amide groups. Thus, in this case we found intimate interactions between the amide and carboxylate groups, which results in a new electronic transition, which is in fact, the lowest energy allowed electronic transition of dipeptides as well as of the carboxylate penultimate ends of peptides and proteins. A number of theoretical papers have recently appeared which verify the existence of charge-transfer transitions both in dipeptides and now also in polypeptides with linked amide groups.^{9,10} The existence of these types of transitions should impact our understanding of peptide electronic excited states, peptide spectroscopy, and the phenomenology of electron transfer in peptides and proteins.

To further probe electronic interactions between coupled amides, we have examined electronic coupling between the linked primary and secondary amide groups of *N*-acetylglyci-

* To whom correspondence should be addressed. Phone: 412-624-8570. Fax: 412-624-0588. E-mail: asher+@pitt.edu.

(1) Murrell, J. N. *The Theory of the Electronic Spectra of Organic Molecules*; Chapman and Hall Ltd.: New York, 1971; pp 47–269.

(2) Scholes, G. D.; Ghiggino, K. P. *J. Phys. Chem.* **1994**, *98*, 4580–4590.

(3) Moffit, W. *J. Chem. Phys.* **1956**, *25*, 467–478.

(4) Woody, R. W. *Circular Dichroism and the Conformational Analysis of Biomolecules*; Fasman, G. D., Ed.; Plenum Press: New York, 1996; pp 25–67 and references therein.

(5) Moffit, W. *Proc. Natl. Acad. Sci. U.S.A.* **1956**, *42*, 736–746.

(6) Brahms, J.; Pilet, H.; Damany, H.; Chandrasekharan, V. *Proc. Natl. Acad. Sci. U.S.A.* **1968**, *60*, 1130–1137.

(7) Chen, X. G.; Li, P.; Holtz, J. S. W.; Chi, Z.; Pajcini, V.; Asher, S. A.; Kelly, L. A. *J. Am. Chem. Soc.* **1996**, *118*, 9705–9715.

(8) Pajcini, V.; Chen, X. G.; Bornett, R. W.; Geib, S. J.; Li, P.; Asher, S. A.; Lidiak, E. G. *J. Am. Chem. Soc.* **1996**, *118*, 9716–9726.

(9) Serrano-Andrés, L.; Fülcher, M. P. *J. Am. Chem. Soc.* **1996**, *118*, 12200–12206.

(10) Serrano-Andrés, L.; Fülcher, M. P. *J. Am. Chem. Soc.* **1998**, *120*, 10912–10920.

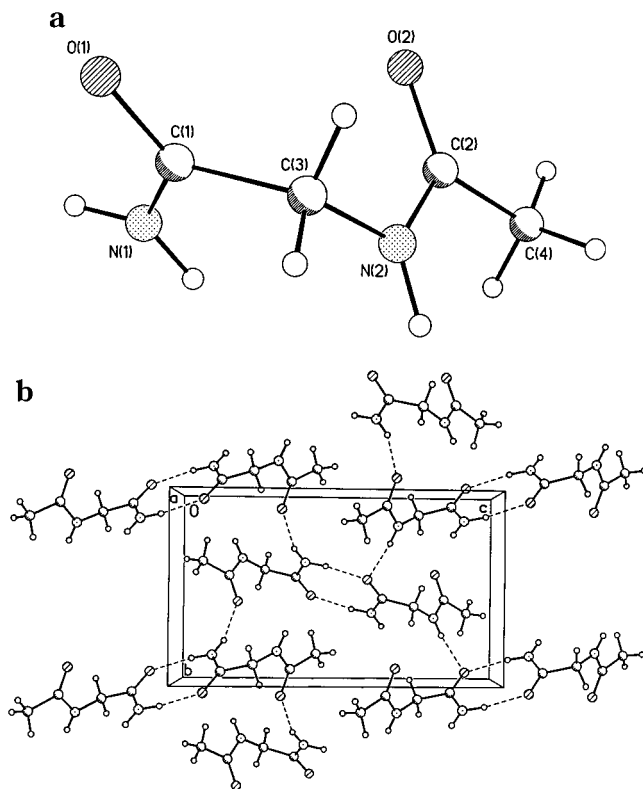


Figure 1. (a) Geometry of *N*-acetylglycinamide (NAGA) obtained from the crystal structure and (b) structure and orientation of the four NAGA molecules within the unit cell, showing the hydrogen-bonding network.

namide ($\text{CH}_3\text{CONHCH}_2\text{CONH}_2$, Figure 1). In a manner essentially identical to our glycyl-glycine studies, we used absorption spectroscopy to measure the oscillator strengths of the *N*-acetylglycinamide (NAGA) 180–200-nm transitions and have determined the transition moment orientations by using polarized preresonance single-crystal Raman spectroscopy.⁸ By comparing the electronic transitions of NAGA to those of the isolated primary and secondary amides we are able to directly determine the nature of the electronic coupling between the two amide fragments.

Experimental Section

Crystal Growth and Structure Determination. *N*-acetylglycinamide, $\text{CH}_3\text{CONHCH}_2\text{CONH}_2$ (NAGA, Figure 1) was purchased from Aldrich Chemical Co. (purity 97%) and was recrystallized three times from ethanol. Large single crystals ($8 \text{ mm} \times 5.3 \text{ mm} \times 1 \text{ mm}$) were grown by slow evaporation of saturated NAGA ethanol solutions.

X-ray diffraction measurements revealed a crystal structure identical to that of Puliti et al.,¹¹ which is monoclinic, of space group $P2_1/n$ (C_{2h}^5) with four molecules per unit cell (Figure 1). Unit cell dimensions are $a = 5.349(4) \text{ \AA}$, $b = 8.065(5) \text{ \AA}$, $c = 13.675(7) \text{ \AA}$, with $\beta = 93.23(5)^\circ$. We redetermined the crystal structure from our X-ray data. The amide conformation of NAGA in the crystal is similar to that which occurs in a type I β -turn in peptides and proteins (NAGA Ramachandran angles $\Phi = -70^\circ$ and $\Psi = -30^\circ$, while typical type I β -turns have $\Phi = -60^\circ$ and $\Psi = -30^\circ$).¹² These angles are also not far from that of an α_R structure.

The NAGA molecules occur in an interconnected intermolecular hydrogen-bonding network. For example, the oxygen of the primary amide is simultaneously hydrogen bonded to the N–H groups of the adjacent primary and secondary amides. The oxygen of the secondary amide is only hydrogen bonded to the primary amide N–H.

(11) Puliti, R.; Mattia, C. A.; Barone, G.; Giancola, C. *Acta Crystallogr.* **1989**, *C45*, 1554–1557.

(12) Creighton, T. E. *Proteins. Structure and Molecular Properties*; W. H. Freeman and Co.: New York, 1996; pp 225–226.

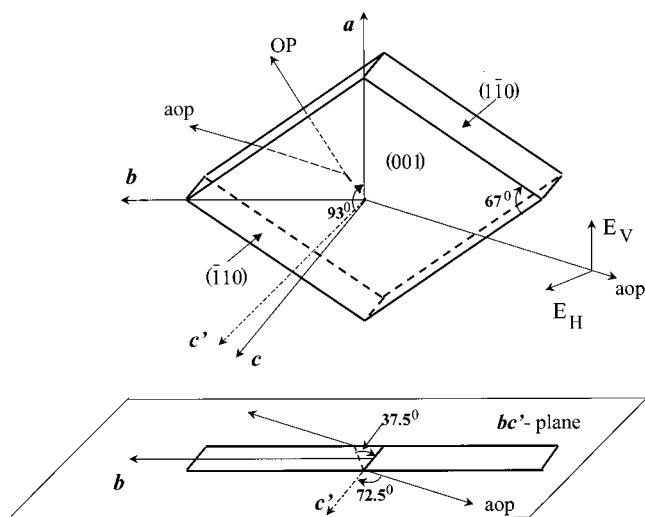


Figure 2. Orientation of NAGA crystal faces relative to the crystal a , b , and c axes. Also shown is the orientation of the c' axis, which is defined to be normal to the a and b axes. The optic axis OP is shown within the crystal, as is the apparent optic axis (aop) outside the crystal. Excitation must occur along “aop” outside the crystal for light to propagate along OP within the crystal.

We used the X-ray crystallography precession method to index the thin NAGA rhombus crystal face (Figure 2).¹³ The large crystal face was normal to the (001) direction, while the four edge faces were indexed as the (110), ($\bar{1}\bar{1}0$), ($\bar{1}10$), and ($1\bar{1}0$) planes. This result is consistent with the relative angles observed between the crystal faces; rhombus face angles of 67° and 113° occur, since $a/b = \tan(67^\circ/2)$. The bisector of the acute angle is the crystallographic b axis, and the bisector of the obtuse angle is the crystallographic a axis.

We determined the crystal optic axes in the visible spectral region by measuring the principal refractive indices $n_\alpha < n_\beta < n_\gamma$, by employing the immersion method, where the refractive indices of a small crystal (of the same morphology as the large crystal) were compared with that of a series of liquids using a microscope.¹⁴ To avoid dissolution of the crystal we used mixtures of hexane, cyclohexane, benzene, and carbon disulfide to obtain refractive indices between 1.375 and 1.628. We found that $n_\alpha = 1.539$, $n_\beta = 1.559$, and $n_\gamma = 1.572$.

We found that for visible light, the three crystallographic axes have refractive indices of $n_c = n_\alpha = 1.539$, $n_a = n_\beta = 1.559$, and $n_b = n_\gamma = 1.572$ and that optic axes lie in the bc (or bc') plane,¹⁵ which is perpendicular to the intersection of an ellipse of semiaxes n_b , n_c , with a circle of radius n_a . For visible light the optic axis makes an angle of 38.4° to the c axis.¹⁶ To transmit visible light from the air along this optic axis ($n_a = 1.559$) within the crystal requires that light be incident onto the crystal at an angle of 75.5° from the perpendicular to the (001) face. This will cause it to refract onto the optic axis inside the crystal.

We expect that the optic axis orientations for 244-nm light is close to our observed orientations of the visible wavelength optic axes. This is reasonable, since we previously demonstrated that the amide $\pi \rightarrow \pi^*$ transitions dominate both the visible and UV optical properties,¹⁷ and relatively little change in orientation of the optic axis occurred between the UV and visible spectral region for glycyl-glycine.⁸ We searched for the actual optical axis orientation in the UV by searching manually for the angle that gave essentially identical 244-nm HV and VH near-resonance Raman spectra. This occurred at an external incident angle of 72.5° to the perpendicular to the (001) face. This external angle in

(13) Buerger, M. J. *The Precession Method in X-ray Crystallography*; John Wiley & Sons: New York, 1964; Chapter 6, pp 69–91.

(14) Bunn, C. W. *Chemical Crystallography*; Clarendon Press: Oxford, 1961; Chapter 3, pp 64–94.

(15) We measured n_c . Since the angle between the c and c' axes is only 3° , we consider n_c and $n_{c'}$ identical.

(16) This angle is equal to $\tan^{-1}(y/x)$, where x and y are the solution of the system of equations $x^2 + y^2 = 1.559^2$ and $x^2/1.572^2 + y^2/1.539^2 = 1$.

(17) Dudik, J. M.; Johnson, C. R.; Asher, S. A. *J. Phys. Chem.* **1985**, *89*, 3805–3814.

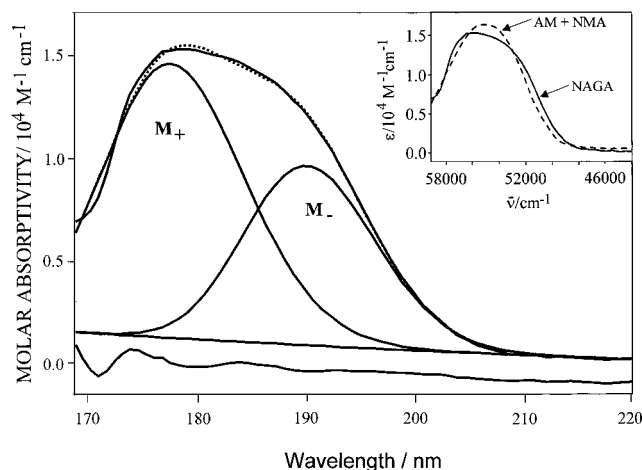


Figure 3. UV absorption spectra of an aqueous solution of *N*-acetylglycinamide (NAGA, 73 mM) and decomposition of the band into two components at 178 and 189 nm. The dotted line is the fitted curve. The inset compares the NAGA absorption spectrum to the sum of acetamide (AM) and *N*-methylacetamide (NMA) spectra. The high-frequencies side of AM and NMA bands are obtained by reflecting the low-frequencies side around ν_{MAX} .

air indicates that the crystal optic axis occurs at an internal angle of $\omega = 37.5^\circ \pm 3^\circ$ to the normal to the (001) surface, for the reasonable range of values of $n_a = 1.567 \pm 0.10$.

Spectroscopic Measurements. The spectroscopic instrumentation and the methodology used to obtain polarized-oriented single-crystal Raman spectra are described in detail elsewhere.⁸ To avoid crystal birefringence, we excited the crystal along the apparent optic axis in air (72.5° from the perpendicular to the (001) face, see Figure 2). In contrast to our previous glycyglycine single-crystal measurements,⁸ in the NAGA crystal the *a* crystallographic axis is the axis of intermediate refractive index, and the *b* axis is the obtuse bisectrix.¹⁸ Thus, the two optic axes are related by a C_2 symmetry operation around the *b* symmetry axis. Spectra collected with the exciting light propagating parallel to each optic axis gives essentially identical data for identical polarizations in the NAGA crystal; the *c* crystallographic axis is almost perpendicular to the *a* crystallographic axis. Thus, we collected all of the polarized Raman data by exciting only along one of the optic axes. In one series of the measurements, we kept the *a* axis vertical, and in the other series, we rotated the crystal clockwise around the optic axis by an angle of 30° (the *a* axis occurs at an angle of 30° to the vertical direction of our laboratory frame).

We measured the vacuum UV absorption spectra of ~ 75 mM aqueous solutions of NAGA, NMA, and AM down to 170 nm at the National Synchrotron Light Source at Brookhaven National Laboratory by using the pseudoabsorption technique.¹⁹

Results and Discussion

1. NMA, AM, and NAGA Electronic Transition Moments.

We directly determined the magnitude of the NAGA, NMA, and AM dipole transition moments from their aqueous solution absorption spectra (Figures 3 and 4). These AM and NMA spectra are reliable for wavelengths above 180 nm, but may show artifactual features at shorter wavelengths caused by water absorption contributions. The broad absorption bands show short wavelength shoulders, which derive from higher energy transitions. We estimated the oscillator strengths of the AM (~ 179 nm) and NMA (~ 185 nm) NV_1 transitions by modeling the low-frequency sides of the absorption bands as Gaussians²⁰ of

(18) Wahlstrom, E. E. *Optical Crystallography*; John Wiley & Sons: New York, 1957; pp 223–226.

(19) Sutherland, J. C.; Keck, P. C.; Griffin, K. P.; Takacs, P. Z. *Nucl. Instrum. Methods* **1982**, *195*, 375–379.

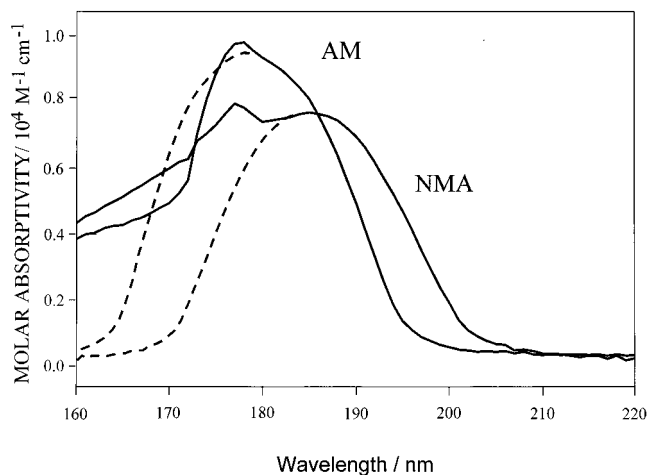


Figure 4. UV absorption spectra of 82 mM aqueous solution of acetamide (AM) and *N*-methylacetamide (NMA). The dotted lines model the high-frequency sides of the absorption spectra by reflecting the low-frequencies sides about ν_{MAX} .

0.262 and 0.198 for AM and NMA, respectively. Thus, the AM and NMA dipole transition moments are $|\mathbf{M}_{\text{AM}}| = 3.16$ D (Debye), and $|\mathbf{M}_{\text{NMA}}| = 2.79$ D. Our experimental values of the AM and NMA oscillator strengths and dipole transition moments are consistent with recent theoretical studies. These studies, however, also demonstrate that the theoretically calculated values are very sensitive to the assumptions used and the theoretical methods employed.²¹

The NAGA broad asymmetric absorption band shown in Figure 3 can be decomposed into two Gaussian bands in the frequency domain, located at ~ 178 nm and ~ 189 nm, which are labeled as \mathbf{M}_+ and \mathbf{M}_- , respectively. These Gaussian bands yield oscillator strengths of $f(\mathbf{M}_+) = 0.290$ and $f(\mathbf{M}_-) = 0.168$ and dipole transition moments of $|\mathbf{M}_+| = 3.32$ D and $|\mathbf{M}_-| = 2.60$ D.^{20,21} The square of the transition moment ratio is $|\mathbf{M}_+|^2/|\mathbf{M}_-|^2 = 1.63$. The inset in Figure 3 compares the NAGA absorption spectrum to the sum of the AM and NMA absorption spectra. The spectral differences indicate electronic interactions between the two NAGA amide fragments. Although there is essentially no difference in the first moment of the NAGA absorption band ($54\,962\text{ cm}^{-1}$) compared to the oscillator strength-weighted first moment of the sum of the NMA and AM absorption spectra ($55\,131\text{ cm}^{-1}$), band shape changes are clearly evident; the \mathbf{M}_+ and \mathbf{M}_- bands are split by a larger amount than are the NV_1 NMA and AM bands (vide infra).

2. Raman Band Assignments. The Raman spectra of NAGA in aqueous solution (Figure 5) can be assigned by analogy to the Raman spectra of NMA^{17,22} and AM.¹⁷ The Raman spectra of NMA shows an amide III (A-III) band at 1313 cm^{-1} (Figure 5a), whose 244-nm Raman cross section is 0.96 mbarn/

(20) (a) Birks, J. B. *Photophysics of Aromatic Molecules*; Wiley-Interscience: London, 1970; pp 44–54. (b) Cantor, C. R.; Schimmel, P. R. *Biophysical Chemistry*; W. H. Freeman and Company: San Francisco, 1980; Part II, pp 356–405.

(21) (a) Hirst, J. D.; Hirst, D. M.; Brooks, C. L., III. *J. Phys. Chem. A* **1997**, *101*, 4821–4827. (b) Besley, N. A.; Hirst, J. D. *J. Phys. Chem. A* **1998**, *102*, 10791–10797. (c) Manning, M. C.; Woody, R. W. *Biopolymers* **1991**, *31*, 569–586. (d) Serrano-Andrés, L.; Fülischer, M. P. *J. Am. Chem. Soc.* **1996**, *118*, 12190–12199.

(22) (a) Chen, C. G.; Asher, A. S.; Schweitzer-Stenner, R.; Mirkin N. G.; Krimm, S. *J. Am. Chem. Soc.* **1995**, *117*, 2884–2895. (b) Chen, C. G.; Schweitzer-Stenner, R.; Asher, A. S.; Mirkin N. G.; Krimm, S. *J. Phys. Chem.* **1995**, *99*, 3074–3083. (c) Chen, C. G.; Schweitzer-Stenner, R.; Mirkin N. G.; Krimm, S.; Asher, A. S. *J. Am. Chem. Soc.* **1995**, *116*, 11141–11142.

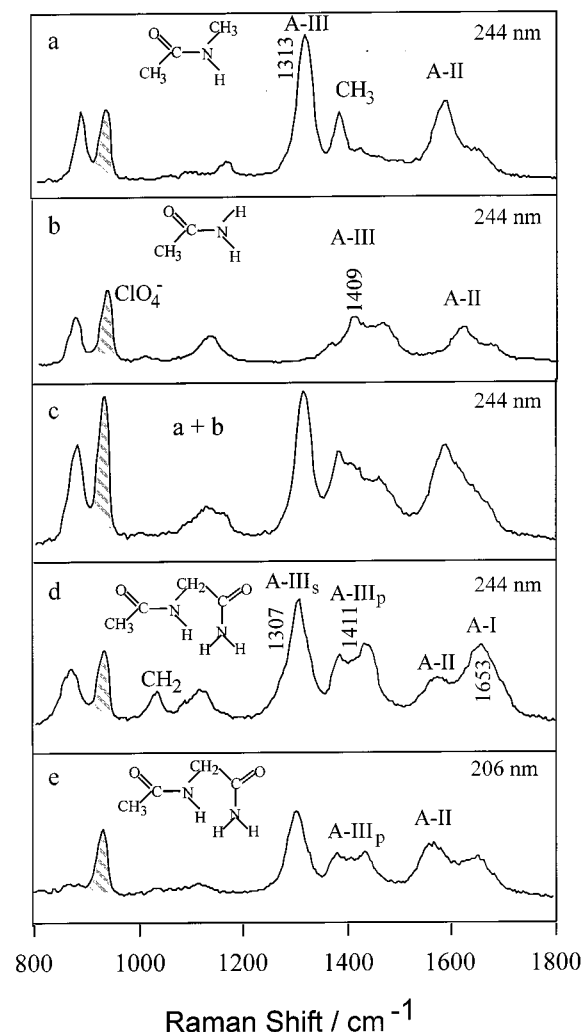


Figure 5. Aqueous solution-phase 244-nm excited Raman spectra of (a) *N*-methylacetamide (NMA), (b) acetamide (AM), (c) sum of spectra a and b, (d) NAGA excited at 244 nm, and (e) NAGA excited at 206 nm. Excitation power was 7.5 mW (244 nm) and 1.0 mW (206 nm); spectral resolution, 12 cm^{-1} (244 nm) and 11 cm^{-1} (206 nm); spectral accumulation time, 50 s (244 nm) and 180 s (206 nm); sample concentrations, 0.4 mM (244 nm) and 5 mM (206 nm). The shaded peak at 932 cm^{-1} derives from the symmetric stretch of the perchlorate internal standard (0.2 M).

molecule·str. The methodologies used to measure the Raman scattering cross sections are described in detail elsewhere.¹⁷ AM shows an A-III band at 1409 cm^{-1} (Figure 5b), whose 244-nm Raman cross section is 0.46 mbarn/molecule·str. A comparison of the 244- and 206-nm NAGA spectra (Figure 5d,e) to the sum of the spectra of NMA and AM (Figure 5c) indicates very similar features.

The NAGA secondary amide A-III band (A-III_s) occurs at 1307 cm^{-1} , while the primary amide A-III (A-III_p) band occurs at 1411 cm^{-1} . The 244-nm Raman cross sections of the NAGA A-III_s and A-III_p bands are 1.17 and 0.45 mbarn/molecule·str, respectively, while the 206-nm cross sections become 114 and 37 mbarn/molecule·str. The 206-nm Raman cross section of the NMA A-III band is 81 mbarn/molecule·str, while the 206-nm Raman cross section of the AM A-III band is 23 mbarn/molecule·str.

A NAGA band similar to the NMA CCH₃ sb at 1380 cm^{-1} is also evident. The 1585 cm^{-1} NMA-like amide II band intensity, which is weak in the 244-nm NAGA spectrum, increases dramatically as the excitation wavelength goes deeper

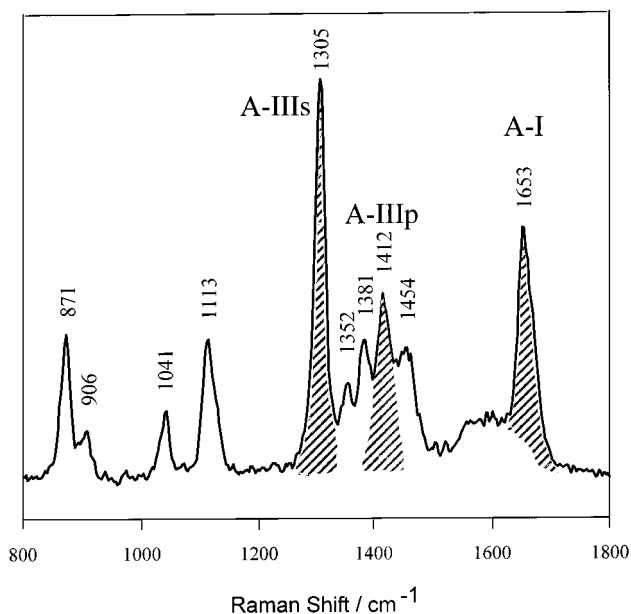


Figure 6. Raman spectrum of NAGA single crystal for 244-nm excitation; the amide III band of the secondary amide (A-III_s) is located at 1305 cm^{-1} , the amide III of the primary amide (A-III_p) is at 1412 cm^{-1} and the unresolved amide I band (A-I) is at 1653 cm^{-1} .

into the UV at 206 nm (Figure 5e). The A-I band shoulder of NMA occurs as a doublet²² at 1626 and at 1645 cm^{-1} , while the A-I band of AM occurs as a shoulder at 1662 cm^{-1} . NAGA in solution at 244-nm excitation shows a strong A-I band, which contains overlapping primary and secondary amide I bands. The 244-nm NAGA A-I band apparent cross section (1.36 mbarn/molecule·str) is increased 4-fold compared to the sum of the 244-nm cross sections of the NMA and AM A-I bands, which are 0.22 and 0.13 mbarn/molecule·str.

These cross-section changes between NAGA and NMA and AM indicate interactions between the two linked NAGA amide electronic transitions. For example, the 89 mbarn/molecule·str 206-nm NAGA A-I band cross section is 1.5 times larger than the sum of the 206-nm A-I band cross sections of NMA (47 mbarn/molecule·str) and AM (14 mbarn/molecule·str).

The 244-nm single-crystal Raman spectrum of NAGA (Figure 6) shows more resolved bands than do the solution phase Raman spectra. The NAGA crystal Raman spectrum is dominated by the A-III_s vibration at $1305 \pm 1 \text{ cm}^{-1}$, while the 1412 cm^{-1} band results from the A-III_p vibration.

The two A-III vibrations of the secondary and primary amides appear to be preserved in NAGA since the NAGA frequencies are very close to those in NMA and AM. This indicates little mixing between these two A-III vibrations. The small NAGA frequency shifts observed between the aqueous solution samples of NAGA, compared to NMA and AM result from modest changes in the vibrational mode composition. Even smaller frequency changes occur for NAGA between the crystal and solution phase. This indicates that for the crystal we may assume an oriented gas model, which assumes little impact of intermolecular vibrational coupling.

The A-I band appears as a single (unresolved) band at $\sim 1653 \pm 3 \text{ cm}^{-1}$ in both the NAGA crystal and in aqueous solution. We were unable to uniquely resolve the two underlying A-I band components. This is probably due to the similarity of frequencies. This also suggests that there is little coupling between the A-I vibrations of the primary and secondary amides; coupling would be expected to increase the splitting between these vibrations.

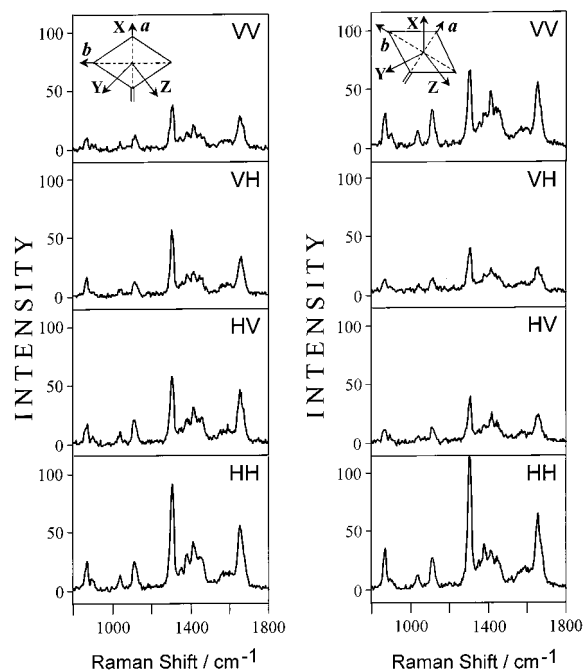


Figure 7. UV Raman spectra of oriented NAGA single crystal excited at 244 nm. The excitation beam propagates along the optic axis Z. The XYZ frame is the laboratory frame with its X axis in the vertical direction V and its Y axis in the horizontal direction H. The exciting light is polarized either vertically (V) or horizontally (H). The Raman scattered light is selected by the analyzer to be either V or H polarized. The abc' frame is the orthogonal crystallographic frame (c' axis, perpendicular to the figure plane, is not shown). In the left panel the axis "a" is parallel to the X axis; in the right panel the axis "a" is inclined 30° to the vertical axis X. The spectra were recorded with accumulation times of 60 s and excitation powers of 1 mW.

The A-II bands of NAGA are much weaker than those of NMA and AM and appear as a weak shoulder of the A-I band. Substitution of the N-H and NH₂ groups by deuterium causes the A-II' bands to appear and the A-II and A-III bands to disappear,^{23,24} in a manner similar to that for NMA and AM (data not shown). Interestingly, the relative intensity of the A-II' to A-I' bands of NAGA in D₂O is much smaller than that for deuterated AM and NMA. Deuterated NAGA shows overlapping, but clearly separate primary and secondary A-II' and A-I' amide bands.

The other nonamide bands of NAGA can be assigned on the basis of the AM and NMA assignments.^{17,22,25} The 871 and 906 cm⁻¹ bands are C-C_α skeletal stretching modes. The band at 1041 cm⁻¹, which has no counterpart in the Raman spectra of AM or NMA but appears in the spectra of Gly-Gly,⁸ is assigned to methylene CH₂ rocking.^{25b} The other rocking band, deriving from the NH₂ group of the primary amide, appears at 1113 cm⁻¹ in the crystal and at 1118 cm⁻¹ in aqueous solution.

The complex band contour centered around 1400 cm⁻¹ is the most difficult region to assign. Clearly, the band at 1381 cm⁻¹ is the CCH₃ symmetric bending observed at this frequency for NMA. The band at 1454 cm⁻¹ is probably the CH₂ bending^{25b} or less likely CCH₃ antisymmetric bending.²²

The UV-polarized Raman spectra of the NAGA crystal are shown in Figure 7. The spectra on the left are measured with a

(23) Sugawara, Y.; Hirakawa, A. Y.; Tsuboi, M. *J. Mol. Spectrosc.* **1984**, *108*, 206–214.

(24) Mayne, L. C.; Hudson, B. *J. Phys. Chem.* **1991**, *95*, 2962–2967.

(25) (a) Krimm, S.; Bandekar, J. *Adv. Protein Chem.* **1986**, *38*, 181–364. (b) Tu, A. *Raman Spectroscopy in Biology*; John Wiley & Sons: New York, 1982; pp 27–31.

Table 1. Correlation Diagram of Molecular and Factor Group

Isolated molecule	Site	Unit Cell
C ₁	C ₁	C _{2h} ⁵
(42A + 3r + 3t)	(42A + 3r + 3t)	(42 + 6r) A _g (R) (42 + 6r) B _g (R) (42 + 5t + 1a) A _u (IR) (42 + 4t + 2a) B _u (IR)

crystallographic axis oriented vertically, and those on the right are taken with a axis inclined 30° to the vertical orientation. The spectra are obtained in the backscattering (−180°) geometry. Thus, the incident light and the Raman scattered light propagate along the same crystal optic axis Z. For each orientation of the crystal we measured four different polarized spectra, HH, HV, VH, and VV. As expected, the HV and VH measurement sets are essentially identical.

3. Crystal Raman Scattering. The NAGA molecule has C₁ symmetry. The 16 atoms in NAGA give rise to 42 internal vibrations, all of which can be Raman and infrared active.^{8,26} The NAGA crystal is monoclinic and of space group of P2₁/n, or in Schönflies notation C_{2h}⁵. The four molecules per unit cell give rise to 168 internal vibrational modes, 12 rotations (r), 9 translation modes (t), and 3 acoustical modes (a) (Table 1). The factor group center of inversion results in only 84 *gerade* Raman active crystal vibrations. One-half belong to the A_g irreducible representation, while the other half belong to the B_g irreducible representation. Very few of these bands are preresonance enhanced with 244-nm excitation, close to the NAGA π → π* transitions.

If 90° or backscattering polarized Raman measurements are made with the incident and scattered light polarizations coincident with the orthogonal crystallographic coordinate system abc' , A_g vibrations of a monoclinic crystal will appear only in the (aa), (bb), (c'c'), and (ac') polarized spectra, while the B_g vibrations will appear only in the (ab) and (bc') polarized spectra.²⁶ The Raman tensors are

$$\alpha^{\text{cry}}(\text{A}_g) = \begin{pmatrix} a & 0 & d \\ 0 & b & 0 \\ d & 0 & c \end{pmatrix}$$

$$\alpha^{\text{cry}}(\text{B}_g) = \begin{pmatrix} 0 & e & 0 \\ e & 0 & f \\ 0 & f & 0 \end{pmatrix} \quad (1)$$

We were unable to measure the Raman spectra of our crystals with the incident and scattered light polarized along the crystallographic coordinate frame because we had to excite along the optic axes.⁸ Only in the case for which X = a did the polarization direction of the incident and scattered light coincide with the a crystallographic axis. Only this VV measurement contains only A_g vibrations. For all other spectra both A_g and B_g vibrations will appear.

The crystal spectra do not show resolved splittings between the A_g and B_g crystal symmetries of each vibration. This probably results from the fact that we are in the oriented gas

(26) Turrell, G. *Infrared and Raman Spectra of Crystals*; Academic Press: London, 1972; pp 56–341.

Table 2. Crystal and Molecular Raman Tensors of the NAGA Amide Vibrations:

A-III (secondary)		
$\alpha^{\text{cry}}(\text{A}_g) = \begin{pmatrix} 0.65 & 0 & -0.58 \\ 0 & 1.08 & 0 \\ -0.58 & 0 & 0.39 \end{pmatrix}$	$\alpha^{\text{cry}}(\text{B}_g) = \begin{pmatrix} 0 & \pm 0.90 & 0 \\ \pm 0.90 & 0 & \pm 0.57 \\ 0 & \pm 0.57 & 0 \end{pmatrix}$	$\alpha^{\text{mol}}(\text{A}) = \begin{pmatrix} 1.80 & 0 & 0 \\ 0 & -0.68 & 0 \\ 0 & 0.00 & 1 \end{pmatrix}$
A-III (primary)		
$\alpha^{\text{cry}}(\text{A}_g) = \begin{pmatrix} 0.69 & 0 & -0.65 \\ 0 & 0.77 & 0 \\ -0.65 & 0 & 0.19 \end{pmatrix}$	$\alpha^{\text{cry}}(\text{B}_g) = \begin{pmatrix} 0 & \pm 0.99 & 0 \\ \pm 0.99 & 0 & \pm 1.02 \\ 0 & \pm 1.02 & 0 \end{pmatrix}$	$\alpha^{\text{mol}}(\text{A}) = \begin{pmatrix} 1.76 & 0 & 0 \\ 0 & -1.11 & 0 \\ 0 & 0 & 1 \end{pmatrix}$
A-I		
$\alpha^{\text{cry}}(\text{A}_g) = \begin{pmatrix} 0.63 & 0 & -0.38 \\ 0 & 0.72 & 0 \\ -0.38 & 0 & 0.68 \end{pmatrix}$	$\alpha^{\text{cry}}(\text{B}_g) = \begin{pmatrix} 0 & \pm 0.84 & 0 \\ \pm 0.84 & 0 & \pm 0.51 \\ 0 & \pm 0.51 & 0 \end{pmatrix}$	$\alpha^{\text{mol}}(\text{A}) = \begin{pmatrix} 1.54 & 0 & 0 \\ 0 & -0.51 & 0 \\ 0 & 0 & 1 \end{pmatrix}$

model limit due to the small intermolecular interactions; the A_g and B_g crystal symmetries of each NAGA vibration have essentially identical frequencies.

The observed polarized crystal Raman intensities are given by

$$I_{\rho\sigma} = A(|\mathbf{e}_\rho^T \alpha^\Omega(\text{A}_g) \mathbf{e}_\sigma|^2 + |\mathbf{e}_\rho^T \alpha^\Omega(\text{B}_g) \mathbf{e}_\sigma|^2) \quad (2)$$

The \mathbf{e}_ρ and \mathbf{e}_σ are unit vectors parallel to the exciting and scattered electrical fields, respectively; T stands for the transpose of the vector \mathbf{e}_ρ ; and A is a proportionality constant. $\alpha^\Omega(\text{A}_g)$ and $\alpha^\Omega(\text{B}_g)$ are the Raman tensors of the A_g and B_g vibrations in the laboratory frame. These differ from the $\alpha^{\text{cry}}(\text{A}_g)$ and $\alpha^{\text{cry}}(\text{B}_g)$ tensors in the crystallographic frame, but are related to them through the appropriate rotation matrixes $\alpha^\Omega(\text{A}_g) = R^T \alpha^{\text{cry}}(\text{A}_g) R$, etc., where R is the orthogonal rotation matrix. (See Appendix.)

The intensity of a polarized Raman band measured in the crystallographic frame is proportional to the sum of squares of the values of the $\alpha^{\text{cry}}(\text{A}_g)$ and $\alpha^{\text{cry}}(\text{B}_g)$ Raman tensor elements ($a, b, c, d, e, \text{ or } f$). Since the factor group symmetry operations leave these elements unchanged or change only their signs,³ each molecule of the crystal unit cell contributes identically at the intensity level to the polarized oriented Raman spectra taken in the crystallographic frame.

4. NAGA Amide Raman Tensors and PART Orientations. We can relate the crystal Raman intensities measured in the laboratory frame to the tensor elements in the crystallographic frame (see Appendix). We can then relate the tensor elements in the crystallographic frame to the molecular diagonal Raman tensor components, whose axes lie along the principal axis of the molecular Raman tensor,⁸ i.e., the Principal Axis of the Raman Tensor (PART).

We curve-fit the polarized crystal Raman bands by using Lorentzian functions. We calculated the peak areas of the amide I band, and of the amide III bands of the secondary and primary amides at 1653, 1305, and 1413 cm^{-1} . These values were used to calculate the Raman tensor and the PART orientations of the A-I, A-IIIs, and A-IIIp bands of NAGA in the crystal.

Equations A8a–f in the Appendix relate the observed Raman intensities for the two crystal orientations to the Raman tensor elements in the crystallographic frame, $\alpha^{\text{cry}}(\text{A}_g)$ and $\alpha^{\text{cry}}(\text{B}_g)$. For the first crystal orientation we have $I_{VV}(1) = I_{XX}(1)$, $I_{VH}(1)$

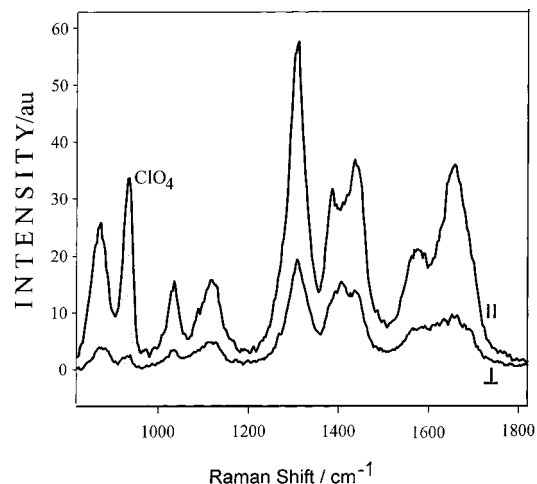


Figure 8. Parallel (||) and perpendicular (⊥) polarized 244-nm UV Raman spectra of aqueous solution of NAGA. Excitation power was 7.5 mW; accumulation time, 50 s; concentration, 0.4 M. The shaded peaks derive from the symmetric stretch of the perchlorate internal standard (0.2 M).

$= I_{HV}(1) = I_{XY}(1)$, $I_{HH}(1) = I_{YY}(1)$, and for the second crystal orientation $I_{VV}(2) = I_{XX}(2)$, $I_{VH}(2) = I_{HV}(2) = I_{XY}(2)$, $I_{HH}(2) = I_{YY}(2)$.

We utilized our measured angles of $\omega = 37.5^\circ$ for the orientation of the optic axis, and the measured crystal orientation angle $\xi = 30^\circ$ to calculate the $\alpha^{\text{cry}}(\text{A}_g)$ and $\alpha^{\text{cry}}(\text{B}_g)$ Raman tensors for the A-IIIs, A-IIIp, and A-I vibrations of the NAGA crystal (Table 2). Because the A8 equations are transcendental, second-order expressions, we do not obtain a single unique solution. We can select the unique solution by utilizing the additional information on the Raman tensor elements obtained from depolarization ratio measurements of randomly oriented NAGA molecules dissolved in water.²⁷ We should note, however, that this creates an implicit assumption that insignificant differences occur for the invariants of the NAGA Raman tensor between the crystal and the solution. The measured Figure 8 depolarization ratios are $\rho(\text{A-IIIs}) = 0.35$, $\rho(\text{A-IIIp}) = 0.51$, and $\rho(\text{A-I}) = 0.29$. The 244-nm solution-phase depolarization

(27) (a) Tsuboi, M.; Ikeda, T.; Ueda, T. *J. Raman Spectrosc.* **1991**, *22*, 619–626. (b) Tsuboi, M.; Thomas, G. J., Jr. *Appl. Spectrosc. Rev.* **1995**, *32* (2), 263–299.

ratio of the NMA A-III band is $\rho = 0.33$, while the AM A-III band is $\rho = 0.37$.

The depolarization ratio is related to the symmetric Raman tensor elements by^{28,29}

$$\rho = \frac{3\gamma^2}{45a^2 + 4\gamma^2} \quad (3)$$

where

$$a = \frac{1}{3}(\alpha_{xx} + \alpha_{yy} + \alpha_{zz}) \quad (3a)$$

and

$$\gamma^2 = \frac{1}{2}\{(\alpha_{xx} - \alpha_{yy})^2 + (\alpha_{yy} - \alpha_{zz})^2 + (\alpha_{zz} - \alpha_{xx})^2 + 6(\alpha_{xy}^2 + \alpha_{yz}^2 + \alpha_{zx}^2)\} \quad (3b)$$

where the tensor elements are defined in the molecular frame.

For each vibrational mode we calculated the crystal frame Raman tensor [$\alpha^{\text{molcry}} = \alpha^{\text{cry}}(\text{A}_g) + \alpha^{\text{cry}}(\text{B}_g)$] by appropriately rotating the measured laboratory frame crystal Raman tensors, subject to the constraints given by eqs 3 and our measured ρ values. The molecular diagonal Raman tensor in the PART frame, α^{mol} is related to crystallographic frame Raman tensor, α^{molcry} by

$$\alpha^{\text{molcry}} = \mathbf{R}^T \alpha^{\text{mol}} \mathbf{R} \quad (4)$$

where $\mathbf{R}(\theta, \varphi, \chi)$ is the orthogonal rotation matrix,⁸ θ , φ , and χ being the Euler's angles,²⁹ and

$$\alpha^{\text{mol}} = \begin{pmatrix} \alpha_{xx} & 0 & 0 \\ 0 & \alpha_{yy} & 0 \\ 0 & 0 & \alpha_{zz} \end{pmatrix} = \alpha_{zz} \begin{pmatrix} r_1 & 0 & 0 \\ 0 & r_2 & 0 \\ 0 & 0 & 1 \end{pmatrix} \quad (5)$$

where $r_1 = \alpha_{xx}/\alpha_{zz}$ and $r_2 = \alpha_{yy}/\alpha_{zz}$.

We determined the Raman tensor elements r_1 and r_2 and angles θ , φ , and χ by solving

$$I_{es} = K |e_c^T \mathbf{R}^T \alpha^{\text{mol}} \mathbf{R} e_s|^2 \quad e, s = a, b, c' \quad (6)$$

where the I_{es} values are those determined in the crystallographic frame and are given by the square of the individual a , b , c , d , e , and f elements of the tensors $\alpha^{\text{cry}}(\text{A}_g)$ and $\alpha^{\text{cry}}(\text{B}_g)$; K is a proportionality constant. (See Appendix A of ref 8.) The elements of the rotation matrix \mathbf{R} are the direction cosines, which relate the PART frame to the crystallographic frame.

Table 2 displays the resulting crystallographic frame (α^{cry}) and molecular diagonal frame Raman tensors (α^{mol}) for the primary and secondary amide A-III and A-I bands. These tensors are normalized to $\alpha^{\text{mol}}_{zz} = 1$. The orientations of the 244-nm excited A-III and the A-I Raman band PARTs are given in Table 3. The most striking feature is that the major axes of the Raman tensors (MARTs) of the amide A-III and A-I Raman bands lie well out of the amide plane. This is in clear contrast to the in-plane orientations expected for the MARTs in the case of isolated amides.^{8,27} The MART of the A-III_s lies 46° out of the secondary amide plane, while the A-III_p MART is 22° out of the primary amide plane. The A-I vibration MART (which is a weighted average from the linked secondary and primary

Table 3. (a) Crystal and (b) Molecular Orientations of the Principal Axes of the *N*-Acetylglycinamide Raman Tensor^a

(a) Crystal Orientations									
angle between PART and	A-III (secondary)			A-III (primary)			A-I		
	<i>x</i>	<i>y</i>	<i>z</i>	<i>x</i>	<i>y</i>	<i>z</i>	<i>x</i>	<i>y</i>	<i>z</i>
<i>a</i> axis	54	144	85	58	143	73	51	139	80
<i>b</i> axis	52	59	53	59	55	60	52	51	62
<i>c'</i> axis	58	73	142	47	79	135	62	79	150
(b) Molecular Orientations									
angle between PART and	A-III (secondary)			A-III (primary)			A-I		
	<i>x</i>	<i>y</i>	<i>z</i>	<i>x</i>	<i>y</i>	<i>z</i>	<i>x</i>	<i>y</i>	<i>z</i>
secondary amide plane	46	41	-14	54	36	-3	52	32	-18
secondary CO bond	130	41	84	126	36	87	125	35	92
secondary CN bond	83	118	151	76	114	152	84	127	143
primary amide plane	-16	28	57	-22	27	54	-15	38	48
primary CO bond	140	66	119	129	59	126	135	66	125
primary CN bond	26	65	87	24	71	75	20	70	88

^a The angles are given in degrees and have a maximum likely error of $\pm 3^\circ$. These orientations are obtained from 244-nm excitation Raman measurements of a *N*-acetylglycinamide (NAGA) crystal.

amides) lies 52° and 15° out of secondary and primary amide planes, respectively.

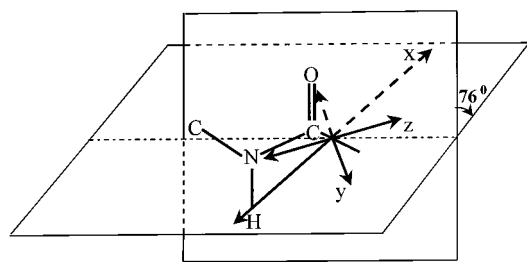
For simple cases of isolated amides such as NMA, formamide and propanamide the A-III vibrational enhancements are dominated by the ~ 185 -nm amide $\pi \rightarrow \pi^*$ (NV_1) transition even far from resonance.¹⁷ In this case the A-III MART would be parallel to the amide $\pi \rightarrow \pi^*$ electronic transition moment, which lies in the amide plane.⁸ In the more general case, with preresonance excitation, small contributions from other transitions can occur to cause the MART to orient slightly off of the direction of the dominant dipole transition moment. The fact that the NAGA MARTs lie significantly out of the amide planes indicates that the two NAGA amide $\pi \rightarrow \pi^*$ (NV_1) transitions are involved in the enhancement, and thus, these different electronic transitions are intimately coupled.

Figure 9 shows the orientations of the NAGA PARTs of the primary and secondary A-III vibrations relative to their respective amide planes. The amide planes lie in the plane of the page. The PART component which lies closest to the amide plane (but not in it) is drawn as a completely solid line. The two other PART components lie in a plane, which forms an angle of 76° to the secondary amide plane and 68° to the primary amide plane. The lengths of the PART axes are proportional to the absolute values of the Raman tensor elements. An important feature is that similar PART orientations occur for both the primary and secondary amide III bands as well as for the amide I band (Table 3). The trace of the secondary amide A-III vibration Raman polarizability tensor is less anisotropic than that of the primary amide (Table 2), which accounts for its smaller solution depolarization ratio compared to that of the primary amide A-III vibration.

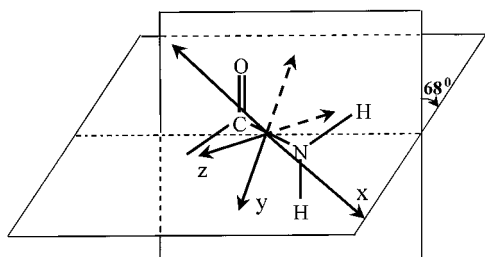
5. NAGA Molecule Electronic Transition Moment Orientations. We can utilize the NAGA UV preresonance Raman tensor data to determine the NAGA electronic transition moment orientation(s).⁸ The NAGA dipeptide has linked primary and secondary amides separated by a methylene group. We begin our analysis by assuming that we can understand the NAGA electronic transitions by considering interactions solely between the adjacent two $\pi \rightarrow \pi^*$ (NV_1) electronic transitions of the secondary and primary amides, which are similar to those of NMA and AM. We include only these lowest energy strongly

(28) Long, D. A. *Raman Spectroscopy*; McGraw-Hill: New York, 1977; pp 46–58.

(29) Wilson, E. B., Jr.; Decius, J. C.; Cross, P. C. *Molecular Vibrations*; Dover: New York, 1980; pp 285–286.



A-III (secondary)



A-III (primary)

Figure 9. Orientations of the principal axes of the Raman tensor (PART) for the NAGA primary and secondary A-III bands relative to their respective amide planes. The respective amide planes lie in the plane of the page. None of the axes lie in the amide plane. The PART component, which is the closest to the amide plane, is drawn as a completely solid line. The perspective plane contains the two other PART components. The lengths of the axes are proportional to the magnitudes of the Raman tensor values. The z axis length equals unity for both bands as we have normalized the tensors with $\alpha_{zz} = 1$. The actual magnitude of α_{zz} is different for secondary and primary A-III bands.

allowed transitions because we have shown that these transitions dominate the amide band preresonance Raman enhancements for excitation from the visible down to 184 nm.^{17,22,30}

The Raman intensities are proportional to the modulus squared values of the polarizability tensor elements, which are in turn determined by the coupling between vibrational and electronic motion within the entire manifold of excited vibronic states. The KHD description of Raman scattering from the i to j vibrational levels of a normal mode of the ground electronic state 0 is^{31–33}

$$(\alpha_{\rho\sigma})_i^j = \frac{1}{hc} \sum_{n,k} \left[\frac{\langle 0j | \mathbf{e}_\rho \cdot \mathbf{M} | nk \rangle \langle nk | \mathbf{e}_\sigma \cdot \mathbf{M} | 0i \rangle}{\bar{\nu}_{nk} - \bar{\nu}_{0i} - \bar{\nu}_L - i\gamma_{nk}} + \frac{\langle 0j | \mathbf{e}_\sigma \cdot \mathbf{M} | nk \rangle \langle nk | \mathbf{e}_\rho \cdot \mathbf{M} | 0i \rangle}{\bar{\nu}_{nk} - \bar{\nu}_{0j} + \bar{\nu}_L - i\gamma_{nk}} \right] \quad (7)$$

where the summation occurs over the electronic excited states, n and their vibrational levels, k . $\bar{\nu}_{nk}$, $\bar{\nu}_{0i}$, and $\bar{\nu}_{0j}$ are the frequencies (cm^{-1}) of states $|nk\rangle$, $|0i\rangle$, and $|0j\rangle$, respectively. $\bar{\nu}_L$ is the frequency of the exciting light; γ_{nk} is the homogeneous line width of each vibronic state (cm^{-1}); and \mathbf{e}_ρ and \mathbf{e}_σ are the

(30) Asher S. A.; Li, P.; Chi, Z.; Schweitzer-Stenner, R.; Mirkin, N. G.; Krimm, S. *J. Phys. Chem. A* **1997**, *101*, 3992–3994.

(31) Placzek, G. *Handbuch der Radiologie*, Marx, E., Ed.; Akademische Verlagsgesellschaft: Leipzig, Germany, 1934; Vol. IV, 2, pp 209–374. (Available in English translation, UCRL-trans-256. US Atomic Energy Comm., Div. Techn. Inform., 1962).

(32) Albrecht, A. C. *J. Chem. Phys.* **1961**, *34*, 1476–1484.

(33) Ting, C. H. *Spectrochim. Acta* **1968**, *24A*, 1177–1189.

unit vectors parallel to the exciting and scattered light polarizations. \mathbf{M} is the electric dipole moment operator.

The Born–Oppenheimer approximation factors the electronic and vibrational wave functions. Thus, in the preresonance regime eq 7 becomes³³

$$(\alpha_{\rho\sigma})_i^j = \frac{1}{hc} \sum_n \frac{\langle 0 | \mathbf{e}_\rho \cdot \mathbf{M} | n \rangle \langle n | \mathbf{e}_\sigma \cdot \mathbf{M} | 0 \rangle}{\bar{\nu}_{n0} - \bar{\nu}_{0i} - \bar{\nu}_L} \left(\sum_k \langle 0j | nk \rangle \langle nk | 0i \rangle \left(1 - k \frac{\bar{\nu}'_n}{\bar{\nu}''_n} + k^2 \frac{\bar{\nu}'_n{}^2}{\bar{\nu}''_n{}^2} - \dots \right) \right) \quad (8)$$

where the second term of eq 7 and γ_{nk} are neglected in our preresonance case. $\bar{\nu}'_n$ is the frequency of the Raman active vibration in excited state n . Thus $\bar{\nu}_{nk} = \bar{\nu}_{n0} + k\bar{\nu}'_n$ and $\bar{\nu}''_n = \bar{\nu}_{n0} - \bar{\nu}_{0i} - \bar{\nu}_L$. For preresonance excitation, $\bar{\nu}'_n$ is significantly smaller than $\bar{\nu}''_n$; thus, we include the first two terms of the binomial expansion (eq 8).

The first term of the Franck–Condon summation over k is equal to unity for $j = i$ and is responsible for the Rayleigh scattering. This term equals zero for the Raman transition $i = 0$ to $j = 1$. The second term^{33,34} equals $(\delta_n/\sqrt{2})(\bar{\nu}'_n/\bar{\nu}''_n)$, while the third term turns out to be $(\delta_n/\sqrt{2})(\delta_n^2 + 1)(\bar{\nu}'_n{}^2/\bar{\nu}''_n{}^2)$, where δ_n is the dimensionless displacement of excited state n relative to the ground state along the normal coordinate of the Raman active vibration. Thus, eq 8 for the Raman transition $i = 0$ to $j = 1$ can be written

$$(\alpha_{\rho\sigma})_0^1 = \frac{1}{hc} \sum_n \frac{\langle 0 | \mathbf{e}_\rho \cdot \mathbf{M} | n \rangle \langle n | \mathbf{e}_\sigma \cdot \mathbf{M} | 0 \rangle}{\bar{\nu}_{n0} - \bar{\nu}_{00} - \bar{\nu}_L} \left[-\frac{\delta_n \bar{\nu}'_n}{\sqrt{2} \bar{\nu}''_n} + \frac{\delta_n}{\sqrt{2}} (\delta_n^2 + 1) \frac{\bar{\nu}'_n{}^2}{\bar{\nu}''_n{}^2} - \dots \right] \quad (9)$$

The values of δ_n , $\bar{\nu}'_n$, and $\bar{\nu}''_n$ for each vibrational normal mode generally differ between the different n excited states. We relate the values of δ_n , $\bar{\nu}'_n$, and $\bar{\nu}''_n$ for the NMA A-III vibration enhanced by the NV_1 transition to the NAGA secondary amide A-III vibration enhanced by the coupled electronic transitions in NAGA by solving simultaneous relations for the Raman intensities measured for two different excitation wavelengths. These expressions utilize the following equations for the A-III Raman intensities for NMA and NAGA:

$$I_{\text{NMA}} = C \left(\frac{M_{\text{NMA}}^2}{\bar{\nu}_{\text{NMA}} - \bar{\nu}_L} \right)^2 \left(\frac{\delta_{\text{NMA}} \bar{\nu}'_{\text{NMA}}}{\bar{\nu}_{\text{NMA}} - \bar{\nu}_L} \right)^2 \quad (10)$$

$$I_{\text{NAGA}} = C \left(\frac{M_+^2}{\bar{\nu}_+ - \bar{\nu}_L} \cdot \frac{\delta_+ \bar{\nu}'_+}{\bar{\nu}_+ - \bar{\nu}_L} + \frac{M_-^2}{\bar{\nu}_- - \bar{\nu}_L} \cdot \frac{\delta_- \bar{\nu}'_-}{\bar{\nu}_- - \bar{\nu}_L} \right)^2 \quad (11)$$

where we neglect the homogeneous line width term for our preresonance excitation, and C is a proportionality constant. The $(\bar{\nu}'_n/\bar{\nu}''_n)^2$ term is ignored because it is small compared to $\bar{\nu}'_n/\bar{\nu}''_n$ for our preresonance 244- and 228.9-nm excitation. $\bar{\nu}_{\text{NMA}}$, $\bar{\nu}_+$, and $\bar{\nu}_-$ are the frequencies of the 0–0 transition ($\bar{\nu}_{n0} - \bar{\nu}_{00}$) of NMA and the two coupled $\pi \rightarrow \pi^*$ transitions of NAGA, respectively. We estimated these values by subtracting 4000 cm^{-1} from the frequency maxima of the absorption bands to account for the absorption Franck–Condon blue shifts of the maxima from the 0–0 transition frequencies, according to the results of Mayne and Hudson.²⁴ We estimate that for NMA in

aqueous solution the NV_1 ($\pi \rightarrow \pi^*$) 0–0 transition frequency band occurs at 50 000 cm^{-1} and that the NAGA coupled transitions occur at 52 000 and 49 000 cm^{-1} .

The measured intensity ratios of the aqueous solution NAGA secondary A-III band to that of the NMA A-III band excited at 244 and 228.9 nm are $I_{\text{NAGA}}/I_{\text{NMA}} = 1.22 \pm 0.04$ and $I_{\text{NAGA}}/I_{\text{NMA}} = 1.15 \pm 0.05$, respectively. The measured values of M_{NMA}^2 , M_+^2 , and M_-^2 are 7.78, 11.02, and 6.76 D^2 , respectively. Thus, we can write the following two simultaneous equations for 244- and 228.9-nm excitation, respectively:

$$0.091\delta_+\bar{\nu}'_+ + 0.106\delta_-\bar{\nu}'_- = 0.106\delta_{\text{NMA}}\bar{\nu}'_{\text{NMA}} \quad (12.1)$$

$$0.160\delta_+\bar{\nu}'_+ + 0.240\delta_-\bar{\nu}'_- = 0.210\delta_{\text{NMA}}\bar{\nu}'_{\text{NMA}} \quad (12.2)$$

All δ 's are expected to have the same sign since they derive from coupling of very similar vibrations to similar electronic transitions. This supposition is confirmed by the fact that the two largest tensor elements of the NAGA crystal for the secondary A-III vibration are of the same the sign.

From eqs 12.1 and 12.2, $\delta_+\bar{\nu}'_+ = 1.5\delta_-\bar{\nu}'_-$ and by using also eq 9 we obtain $\delta_+\bar{\nu}'_+/(\bar{\nu}_+ - \bar{\nu}_L) = (1.05 \pm 0.1)\delta_-\bar{\nu}'_-/(\bar{\nu}_- - \bar{\nu}_L)$ for 244-nm excitation ($\bar{\nu}_L = 41\,000\text{ cm}^{-1}$). This means that the Raman polarizability contributions from each of the two NAGA electronic transitions are very similar for 244-nm excitation. The above result indicates a substantial mixing of the original primary and secondary amide electronic transitions, which results in a smaller A-III Franck–Condon factors within each NAGA molecule excited state compared to what is present in the NMA molecule. Similar results are obtained for the NAGA primary A-III band by comparing it with the AM A-III band; thus, $\delta_+\bar{\nu}'_+ = 1.43\delta_-\bar{\nu}'_-$ and $\delta_+\bar{\nu}'_+/(\bar{\nu}_+ - \bar{\nu}_L) = (1.05 \pm 0.1)\delta_-\bar{\nu}'_-/(\bar{\nu}_- - \bar{\nu}_L)$ for 244-nm excitation.

If these two mixed electronic transitions, M_+ and M_- , dominate the KHD sum over states in eq 8, we can determine their relative transition moment orientations from the experimentally measured Raman tensor elements.^{7,8} A linearly polarized resonant electronic transition in the diagonal frame results in only a single Raman tensor element α_{ii} , where direction i is parallel to the electronic transition moment. If we define α_+ as the NAGA Raman polarizability tensor element derived from electronic transition M_+ in its diagonal frame, and α_- as the tensor element derived from the M_- transition in its diagonal frame, α_+ and α_- are oriented along their respective transition moment directions. If M_+ is parallel to the x_1 axis in the $x_1y_1z_1$ coordinate system and M_- is parallel to x_2 in the $x_2y_2z_2$ system, the Raman tensor elements α_{xx} and α_{zz} in the xyz PART frame of the NAGA crystal are given by^{7,8}

$$\alpha_{xx} + \alpha_{zz} = \alpha_+ + \alpha_- \quad (13)$$

$$\alpha_{xx}\alpha_{zz} = \alpha_+\alpha_- \sin^2\beta \quad (14)$$

where β is the angle between the M_+ and M_- transition moments.

The polarized oriented Raman crystal measurements discussed above determine the values of α_{xx} and α_{zz} . We require an additional relationship to uniquely determine α_+ , α_- , and the angle β . We can utilize the ratio

$$\frac{\alpha_+}{\alpha_-} = \frac{|M_+|^2 (\bar{\nu}_- - \bar{\nu}_L)^2 \delta_+\bar{\nu}'_+}{|M_-|^2 (\bar{\nu}_+ - \bar{\nu}_L)^2 \delta_-\bar{\nu}'_-} \quad (15)$$

to obtain, $\alpha_+/\alpha_- = 1.3$ at 244 nm and $\alpha_+/\alpha_- = 1.0$ at 229 nm. This ratio is reduced to 0.05 at 206.5-nm excitation. In eq 15,

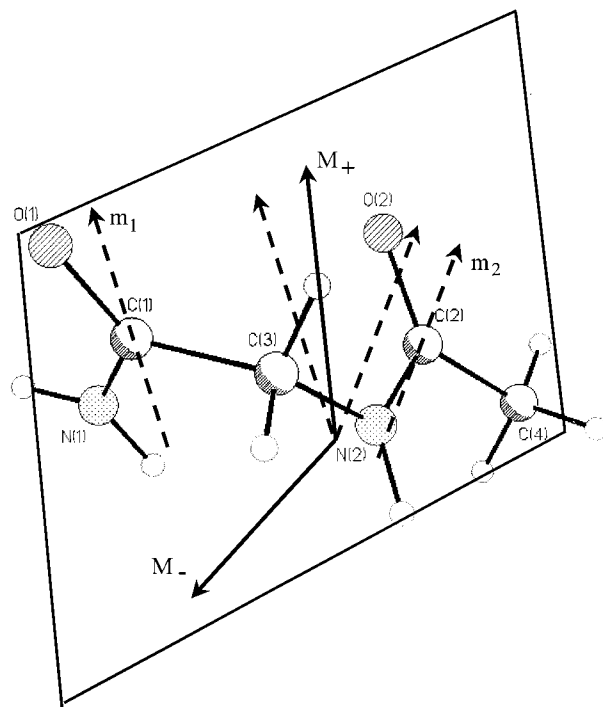


Figure 10. Orientations of NAGA M_+ and M_- dipole transition moments compared to the orientations of the unperturbed NV_1 ($\pi \rightarrow \pi^*$) transition moments of each fragment, m_1 and m_2 . All the transition moments lie in the same plane.

$\bar{\nu}_+ = 52\,000\text{ cm}^{-1}$ and $\bar{\nu}_- = 49\,000\text{ cm}^{-1}$ are the 0–0 transition frequencies of the NAGA M_+ and M_- electronic transition moments.

From these relationships for the secondary amide III vibration we calculate an acute angle β of $75^\circ \pm 4^\circ$ (the obtuse angle is $105^\circ \pm 4^\circ$) between the M_+ and M_- electronic transition moments. We can similarly use the Raman tensor data of the A-IIIp and A-I bands which yield acute β angles of $76^\circ \pm 4^\circ$ and $80^\circ \pm 4^\circ$, respectively (average value of $\beta = 77^\circ \pm 4^\circ$).

The angle ζ between the larger transition moment, M_+ and MART is⁸

$$\zeta = \frac{1}{2} \tan^{-1} \left\{ -\frac{\alpha_- \sin(2\beta)}{\alpha_+ + \alpha_- \cos(2\beta)} \right\} \quad (16)$$

The value of ζ is extremely sensitive to the α_+/α_- ratio, in contrast to the angle β between the transition moments. We calculate that ζ is 4° for A-III, 5° for A-IIIp and 2° for the A-I MART, although given our error analysis it is possible that these angles could be as large as 16° . We conclude that the 244-nm excited Raman spectra NAGA MART orientations of these amide vibrations are almost parallel to the higher frequency M_+ transition moment. The orientations of the NAGA M_+ and M_- transition moments are shown in the Figure 10. The angles between the M_+ and M_- and the isolated amide transition moments are discussed below.

6. Mixing between NAGA Primary and Secondary Amide Transition Moments. NAGA is a dimer of primary and secondary amides. In the crystal these two amide planes are nearly perpendicular with a dihedral angle of 85° . The magnitude of coupling between these two transitions should be related to the relative orientations of their m_1 and m_2 $\pi \rightarrow \pi^*$ (NV_1) electric dipole transition moments.

The NAGA dimer excited states can be modeled as linear combinations of the locally excited amide configurations.³⁵ Thus, if we write the local ground-state wave functions of the primary and secondary amide as π_1 and π_2 and their respective excited

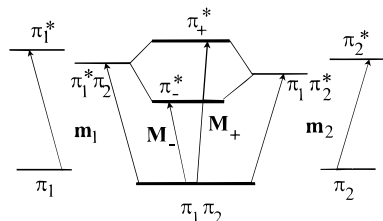


Figure 11. Energy level diagram for coupling of the $\pi\pi^*$ excited states and the respective dipole transition moments in NAGA. $\pi_1\pi_2$ is the dipeptide ground-state wave function, while π_1 and π_2 are the ground states of each isolated amide. $\pi_1^*\pi_2^*$ and $\pi_1\pi_2^*$ are locally excited configurations and π_+^* and π_-^* are the NAGA excited states. \mathbf{M}_+ and \mathbf{M}_- are the NAGA transition moments, while \mathbf{m}_1 and \mathbf{m}_2 are the respective dipole transition moments of the isolated amides.

states as π_1^* and π_2^* , the NAGA dimer excited-state wave functions can be written as

$$\pi_+^* = \cos \alpha (\pi_1^*\pi_2) + \sin \alpha (\pi_1\pi_2^*) \quad (17.1)$$

$$\pi_-^* = \sin \alpha (\pi_1^*\pi_2) - \cos \alpha (\pi_1\pi_2^*) \quad (17.2)$$

where $\pi_1^*\pi_2$ and $\pi_1\pi_2^*$ are the locally excited amide states and α is the mixing parameter (Figure 11), with $0^\circ \leq \alpha \leq 90^\circ$ and $\alpha = 45^\circ$ for identical monomers.

The dimer transition moments $\mathbf{M}_+ = \langle \pi_+^* | \mathbf{M} | \pi_1\pi_2 \rangle$ and $\mathbf{M}_- = \langle \pi_-^* | \mathbf{M} | \pi_1\pi_2 \rangle$ can be written as

$$\mathbf{M}_+ = \cos \alpha \mathbf{m}_1 + \sin \alpha \mathbf{m}_2 \quad (18.1)$$

$$\mathbf{M}_- = \sin \alpha \mathbf{m}_1 - \cos \alpha \mathbf{m}_2 \quad (18.2)$$

where $\mathbf{m}_1 = \langle \pi_1^*\pi_2 | \mathbf{M} | \pi_1\pi_2 \rangle$ and $\mathbf{m}_2 = \langle \pi_1\pi_2^* | \mathbf{M} | \pi_1\pi_2 \rangle$ are the individual amide fragment NV_1 $\pi \rightarrow \pi^*$ dipole transition moments of AM and NMA, respectively, as we will shown below. Their magnitudes are estimated from the absorption spectra of AM and NMA, while their orientations have been experimentally determined from previous single-crystal measurements.^{8,36–38}

For example, our preresonance Raman single-crystal measurements of glycyl-glycine⁸ determined that the secondary amide NV_1 transition moment, \mathbf{m}_2 orients within the amide plane, $-46^\circ \pm 3^\circ$ to the carbonyl bond (positive angles are defined such that the transition moment forms an acute angle to the carbonyl bond on the side containing the N atom of the amide group). Clark's *N*-acetylglucine linear dichroism measurements also found that the secondary amide NV_1 transition moment occurs in the amide plane;²⁸ however, the angle was found to be $-55^\circ \pm 5^\circ$ to the carbonyl bond, which differs by an amount just greater than the experimental uncertainties.

For the primary amide \mathbf{m}_1 orientation, we can use Clark's propanamide result,³⁶ that the NV_1 transition moment orients in the amide plane at $-35^\circ \pm 3^\circ$ from the C=O axis; this value is insignificantly different from the -41° angle measured earlier for myristamide given Peterson and Simpson's likely experimental uncertainties.³⁷

To calculate excitonic interactions between the amide transitions from the measured \mathbf{M}_+ and \mathbf{M}_- magnitudes of isolated

(34) Hutchinson, E. *Phys. Rev.* **1930**, *36*, 410–420.

(35) Förster, Th. *Delocalized Excitation and Excitation Transfer*, Modern Quantum Chemistry, Istanbul Lectures; Sinanoglu, O., Ed.; Academic Press: New York, 1965; Part III, pp 93–137.

(36) Clark, L. B. *J. Am. Chem. Soc.* **1995**, *117*, 7974–7986.

(37) Peterson, D. L.; Simpson, W. T. *J. Am. Chem. Soc.* **1957**, *79*, 2375–2382.

(38) Ward, J. C. *Proc. R. Soc. London* **1955**, *A288*, 205–219.

Table 4. (a) Possible NV_1 Transition Moment Orientations in Primary and Secondary Amides and (b) Interaction Energy U , Mixing Parameter α , and NAGA Transition Moments Magnitudes for Different Orientations of NV_1 Transition Moments in Primary and Secondary Amides

(a)							
angle between C=O bond and	Clark ³⁶ crystal data ^b	Pajcini et al. ⁸ crystal data ^b	corrected by Woody ^{39,b}				
\mathbf{m}_1^d	-35 ± 3						-25
\mathbf{m}_2^d	-55 ± 5	-46 ± 3					-35
(b)							
\mathbf{m}_1 (deg)	\mathbf{m}_2 (deg)	γ^c (deg)	α (deg)	$ \mathbf{M}_+ $ (D)	$ \mathbf{M}_- $ (D)	U (cm^{-1})	$2U/\sin 2\alpha$
-35	-55	97	-22	2.71	3.23	734	2098
-35	-46	90	0	3.16	2.79	686	
-25	-35	80	27	3.28	2.65	881	2172
-25	-40	84	20	3.21	2.73	935	2909
experimental data				3.32	2.60		3270

^a \mathbf{m}_1 is the NV_1 transition moment of the primary amide and \mathbf{m}_2 is the NV_1 transition moment of the secondary amide. They both lie in their amide planes. ^b The angles are given in degrees with positive angles measured toward the N atom of the amide group. ^c γ is the angle between the unperturbed NV_1 transition moments \mathbf{m}_1 and \mathbf{m}_2 in NAGA. The distance between two NAGA chromophores is $R_{12} = 3.16$ Å.

NAGA monomers in aqueous solution, we must relate the transition moment orientations observed in the single crystal to those occurring for NAGA monomers in solution. We assume that the NAGA structure in aqueous solution differs insignificantly from that in the crystal. Even if a number of solution-phase conformers are present, we assume that conformations close to that in the crystal dominates.

Clark³⁶ and Woody³⁹ have argued that the crystal field and crystal excitonic effects significantly alter the transition moment orientations. For example, the gas-phase NV_1 transition moment of the primary amide propanamide has been calculated to occur at -25° from the carbonyl bond, $+10^\circ$ from the observed crystal value.³⁹ Woody also calculated that the secondary amide *N*-acetylglucine NV_1 transition moment occurs at -35° , 20° away from the observed crystal value (Table 4a).³⁹

If \mathbf{m}_1 and \mathbf{m}_2 were oriented at -35° and -46° from their C=O bonds, they would have crystallographic frame direction cosines of (0.765, -0.641 , -0.056) and (-0.608 , -0.743 , 0.278), respectively. In this case the angles between the primary A-III MART and \mathbf{m}_1 and \mathbf{m}_2 would be 26° and 70° , while the angles between secondary A-III MART and \mathbf{m}_1 and \mathbf{m}_2 would be 16° and 75° . If \mathbf{m}_1 is at -25° and \mathbf{m}_2 is at -40° the primary A-III MART would make angles to them of 31° and 67° , while the secondary A-III MART would make angles of 20° and 71° , respectively. The fact that the primary and secondary A-III MARTs are oriented more along \mathbf{m}_1 than \mathbf{m}_2 is associated with the larger NAGA enhancement occurring from the primary amide transition.

We will calculate the amide excitonic interactions using all of the possible \mathbf{m}_1 and \mathbf{m}_2 orientations discussed above. We also examine the possibilities that \mathbf{m}_2 occurs at -40° and -55° from the carbonyl bond (Table 4).

The NAGA transition moments must lie in the plane containing the transition moments of the unperturbed primary and secondary amides. This expectation is also consistent with our determination that the MART of the secondary A-III lies only 2 – 3° out of this plane, while the primary A-III and A-I MARTs lie only $14^\circ \pm 3^\circ$ and $9^\circ \pm 2^\circ$ out of this plane.

(39) Woody, R. W. *Prog. Biophys. Mol. Biol.* **1996**, *65* (Suppl. 1), 57.

However, the second largest z-PARTs clearly lie out of this plane by 29° for the primary A-III band, 36° for secondary A-III band, and 43° for A-I band. This is expected, since the α_{yy} Raman tensor element value is not zero. This suggests that some pre-resonance Raman enhancement also occurs from additional electronic transitions. The similarity of the UV Raman spectra of NAGA to that of AM and NMA suggest that these additional transitions derive from transitions of the individual primary and secondary amides. However, it is also possible that some contribution occurs from new NAGA charge-transfer transitions similar to those calculated recently.¹⁰ It is likely that careful NAGA solution Raman depolarization ratio dispersion measurements could determine the types of transitions contributing to enhancement.

In principle, α can be calculated using eqs 18.1 and 18.2 from the NAGA transition moment magnitudes, $|\mathbf{M}_+|$ and $|\mathbf{M}_-|$, and the AM and NMA transition moments, \mathbf{m}_1 and \mathbf{m}_2 , obtained from aqueous solution absorption spectra. We can obtain from eqs 18.1 and 18.2

$$|\mathbf{M}_+|^2 = \cos^2 \alpha |\mathbf{m}_1|^2 + \sin^2 \alpha |\mathbf{m}_2|^2 + 2 \sin \alpha \cos \alpha |\mathbf{m}_1| |\mathbf{m}_2| \cos \gamma \quad (19.1)$$

$$|\mathbf{M}_-|^2 = \sin^2 \alpha |\mathbf{m}_1|^2 + \cos^2 \alpha |\mathbf{m}_2|^2 - 2 \sin \alpha \cos \alpha |\mathbf{m}_1| |\mathbf{m}_2| \cos \gamma \quad (19.2)$$

where γ is the angle between \mathbf{m}_1 and \mathbf{m}_2 .

Equations 19.1 and 19.2 are not independent and, thus, cannot by themselves be used to determine unique α and γ values. We can, however, calculate possible α values from the list of possible γ values calculated from the possible orientations discussed above (tabulated in Table 4b). We will choose the α -value that gives us the best fit for the \mathbf{M}_+ and \mathbf{M}_- values. We find that α monotonically varies from $\alpha = -22^\circ$ for $\gamma = 97^\circ$, to $\alpha = 27^\circ$ for $\gamma = 80^\circ$. We immediately neglect $\alpha = -22^\circ$ since it lies outside of the acceptable range $0^\circ \leq \alpha \leq 90^\circ$. A value of $\alpha = 0^\circ$ would indicate the absence of excitonic interactions.

We can make further progress by utilizing the observed energy splitting between \mathbf{M}_+ and \mathbf{M}_- to further constrain the possible values of α . The energies of the π^*_{+} and π^*_{-} states are given by³⁵

$$W_{\pm} = \frac{1}{2}(W'_1 + W'_2) \pm (U/\sin 2\alpha) \quad (20)$$

where W'_1 and W'_2 are the energies of the configurations $\pi^*_1\pi_2$ and $\pi^*_2\pi_1$ and $2U/\sin 2\alpha$ is the energy splitting between the π^*_{+} and π^*_{-} states (Figure 11). U is the electric dipole transition moment interaction energy:^{21,35}

$$U = (\mathbf{m}_1 \cdot \mathbf{m}_2) R_{12}^{-3} - 3(\mathbf{m}_1 \cdot \mathbf{R}_{12})(\mathbf{m}_2 \cdot \mathbf{R}_{12}) R_{12}^{-5} \quad (21)$$

where \mathbf{R}_{12} is the vector between the two monomers. In NAGA, we define R_{12} as the distance between C(1) and C(2) (Figure 1), where $R_{12} = 3.16 \text{ \AA}$ and vector \mathbf{R}_{12} has crystal components (1.21, -0.044, -2.92). We assume that the transition dipoles are sufficiently close that we can assume a dielectric constant of one.

Table 4b shows that these calculated splitting energies only approach our 3270 cm^{-1} measured value for $\alpha = 20^\circ$, otherwise the splitting is much too low. This result is consistent with the \mathbf{m}_1 and \mathbf{m}_2 orientations which are close to those Woody suggested would occur for the isolated amides unperturbed by crystal field effects.³⁹ Thus, we tentatively conclude that for

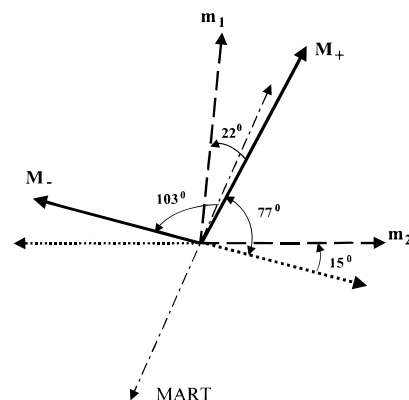


Figure 12. Orientations of NAGA \mathbf{M}_+ and \mathbf{M}_- dipole transition moments and the \mathbf{m}_1 and \mathbf{m}_2 $\pi \rightarrow \pi^*$ transition moments of the isolated chromophores. All moments lie in the plane of the figure. The lengths of the moments are drawn proportional to their magnitudes. The Raman tensor major axes for all amide vibrations (MARTs) lie in this plane, close to the \mathbf{M}_+ moment. Only the A-IIIs MART is shown.

isolated NAGA in aqueous solution \mathbf{m}_1 and \mathbf{m}_2 orient at -25° and -40° to the carbonyl bonds. We must recognize, however, that our use of the point dipole model may be inaccurate at these short distances. In the future we hope to examine these interactions by theoretical calculations that allow us to calculate the interaction using a distributed dipole or monopole approach.

Thus, we find for NAGA in aqueous solution an angle of $\gamma = 84^\circ$ between the unperturbed \mathbf{m}_1 and \mathbf{m}_2 transition moments. From eqs 18.1 and 18.2, we calculate an acute angle between \mathbf{M}_+ and \mathbf{m}_1 of 22° and between \mathbf{M}_- and \mathbf{m}_2 of 15° . This gives rise to an acute angle of 77° (obtuse angle 103°) between the NAGA molecule \mathbf{M}_+ and \mathbf{M}_- transition moments, in agreement with our Raman experimental measurements (see Figure 12). The MART of the secondary A-III vibration lies almost parallel to the NAGA \mathbf{M}_+ transition moment. The degree of mixing of the amide transitions is evident here, since this originally was the primary amide transition.

The orientations of \mathbf{M}_+ , \mathbf{M}_- , \mathbf{m}_1 , and \mathbf{m}_2 are shown within the NAGA molecule in Figure 10, where the plane of the page contains the transition moments. The plane containing \mathbf{M}_+ and \mathbf{M}_- shows dihedral angles with the primary and secondary amide planes of $\sim 80^\circ$ and $\sim 35^\circ$, respectively.

Our calculated $\alpha = 20^\circ$ mixing parameter, indicates excitonic mixing between the secondary and primary amide electronic transitions. For example, \mathbf{M}_- is primarily a secondary amide transition with a $\sim 36\%$ contribution from the primary amide transition moment, while \mathbf{M}_+ is primarily a primary amide transition. The excitonic coupling cause the enhancement from \mathbf{M}_- to decrease due to the negative sign in eq 18.2 for an acute angle between \mathbf{m}_1 and \mathbf{m}_2 . Thus, \mathbf{M}_+ is calculated and is observed to dominate the enhancement of the amide vibrations.

Alternatively we can use a more empirical approach³⁵ (eq 22) to calculate α by estimating the energy splitting W_{\pm} from our experimental NMA and AM transition frequency data:

$$W_{\pm} = \frac{1}{2}(W'_1 + W'_2) \pm [(W'_1 - W'_2)/2 \cos 2\alpha] \quad (22)$$

We obtain a mixing parameter $\alpha = 28.2^\circ$ from the experimentally measured $W_+ - W_- = 3270 \text{ cm}^{-1}$. This argues for stronger mixing between the monomer transitions. The resulting interaction energy $U = 1361 \text{ cm}^{-1}$ is significantly larger than that calculated from dipole-dipole interactions (eq 21) or using

monopoles.⁴⁰ The fact that U exceeds our calculated through-space interaction energies may indicate that through-bond coupling may be also be significant (in the form of mixing with CT transitions,¹⁰ for example). The value of $\alpha = 28.2^\circ$, can be calculated from eq 19 to result in a value of $\gamma = 78^\circ$, essentially identical to that calculated earlier ($\gamma = 77^\circ \pm 4^\circ$).

We anticipate much larger excitonic interactions for peptides in β -sheet structures, for example, where the adjacent secondary amide planes lie almost parallel to one another. Further, there is the additional possibility of interactions between the frontier orbitals of the adjacent amides. These types of interactions, for example, give rise to conjugation in polyenes. This, of course, would be minimized for NAGA, where the amide planes and their π -orbitals are almost perpendicular. We will examine this issue further in dipeptides where the amide planes are more parallel.

Finally, our conclusions concerning the magnitude of exciton mixing between the NAGA primary and secondary amides depends on whether our assumption of the oriented gas model is correct. If, instead, comparable or larger excitonic interactions occur between adjacent NAGA molecules in the unit cell, this will confound our analysis. Our use of the oriented gas model is rationalized by two experimental facts: (1) The primary and secondary amides lie closer to one another in NAGA than do the amides within the unit cell. This proximity should result in a 3-fold larger NAGA intramolecular interaction. (2) The perturbation in the Raman spectra of NAGA compared to the sum of the spectra of AM and NMA is essentially identical for the isolated solution NAGA spectra and the NAGA crystal. Since the vibrational modes remain essentially identical, this indicates that the excited-state perturbations are dominated by the intramolecular exciton interactions present between the amides within each NAGA molecule. Thus, the contributions from intermolecular exciton interactions must be much smaller.

Conclusions

UV preresonance single-crystal Raman measurements have been used to determine the coupling between the amide transitions in *N*-acetylglycinamide (NAGA), a dipeptide of linked secondary and primary amides. We find significant exciton coupling between the secondary and primary amide transitions even though the unperturbed transitions are almost perpendicular to one another ($\gamma = 80^\circ$). The coupled NAGA transition moments are significantly rotated from that which would occur from the individual amide transitions.

We anticipate much larger interactions between the linked amides of peptides and proteins in the more typical cases where the transition moments are more parallel, such as in α -helices and especially in β -sheet peptides where the amide planes are almost parallel. This should result in stronger coupling between adjacent amide electronic transitions and excited states.

Acknowledgment. We gratefully acknowledge support from NIH grant GM30741 and thank Professor Brian M. Craven from the Department of Crystallography for help in indexing the crystal faces. We also thank Dr. Steven J. Geib, the crystallographer of our Chemistry Department for the X-ray redetermination of the crystal structure. We acknowledge the National Synchrotron Light Source at Brookhaven National Laboratory supported by the Office of Basic Energy Science, Office of Science (OS), and United States Department of Energy (US-

DOE) for UV pseudo-absorption measurements using beamline {U9B, U11, X13A} which is supported by the Office of Biological and Environmental Research, OS, and UDOE. We also thank John G. Trunk for his kind help in the UV absorption experiments.

Appendix

Here we relate the Raman tensor elements and the Raman intensities in the crystallographic frame to those measured in the laboratory frame, for our NAGA crystal, which has its optic plane perpendicular to the a crystallographic axis.

In the first set of the measurements, the XYZ laboratory frame is related to the orthogonal crystallographic frame by a rotation of angle ω about the $a = X$ axis. The rotation matrix is

$$\mathbf{R}_X(\omega) = \begin{pmatrix} 1 & 0 & 0 \\ 0 & \cos \omega & \sin \omega \\ 0 & -\sin \omega & \cos \omega \end{pmatrix} \quad (\text{A1})$$

Thus, the Raman tensor in the laboratory system, $\alpha^{\text{lab}(1)}$ for the first set of measurements is given by

$$\alpha^{\text{lab}(1)} = \mathbf{R}_X^T(\omega) \alpha^{\text{cry}} \mathbf{R}_X(\omega) \quad (\text{A2})$$

where α^{cry} is the Raman tensor expressed in the abc' Cartesian crystallographic coordinate system. For the Raman active molecular vibrations of the irreducible representation A_g and B_g , α^{cry} is written as²⁶

$$\alpha^{\text{cry}}(A_g) = \begin{pmatrix} a & 0 & d \\ 0 & b & 0 \\ d & 0 & c \end{pmatrix} \quad (\text{A3})$$

$$\alpha^{\text{cry}}(B_g) = \begin{pmatrix} 0 & e & 0 \\ e & 0 & f \\ 0 & f & 0 \end{pmatrix} \quad (\text{A4})$$

For an A_g vibration, we obtain the following Raman tensor elements in the first XYZ laboratory system:

$$\alpha_{XX}^{(1)} = a \quad \alpha_{XY}^{(1)} = \alpha_{YX}^{(1)} = -d \sin \omega$$

$$\alpha_{YY}^{(1)} = b \cos^2 \omega + c \sin^2 \omega$$

In the same way for a B_g vibration the result is

$$\alpha_{XX}^{(1)} = 0 \quad \alpha_{XY}^{(1)} = \alpha_{YX}^{(1)} = e \cos \omega$$

$$\alpha_{YY}^{(1)} = -f \sin(2\omega)$$

In the second set of measurements, we rotated the crystal around the optic axis Z , by an angle $-\xi$. This means that the new laboratory frame is obtained from the old one by a rotation around Z axis with an angle ξ . Thus, the Raman tensor in the second laboratory frame $\alpha^{\text{lab}(2)}$, is

$$\alpha^{\text{lab}(2)} = \mathbf{R}_Z^T(\xi) \alpha^{\text{lab}(1)} \mathbf{R}_Z(\xi) \quad (\text{A5})$$

with

$$\mathbf{R}_Z(\xi) = \begin{pmatrix} \cos \xi & \sin \xi & 0 \\ -\sin \xi & \cos \xi & 0 \\ 0 & 0 & 1 \end{pmatrix} \quad (\text{A6})$$

From eqs A5 and A2 we have

$$\alpha^{\text{lab}(2)} = \mathbf{R}_Z^T(\xi) \mathbf{R}_X^T(\omega) \alpha^{\text{cry}} \mathbf{R}_X(\omega) \mathbf{R}_Z(\xi) \quad (\text{A7})$$

(40) (a) Tinoco, I., Jr.; Woody, R. W.; Bradley, D. F. *J. Chem. Phys.* **1963**, *38*, 1317–1325. (b) Woody, R. W. *J. Chem. Phys.* **1968**, *49*, 4797–4806.

Equation A7 gives the following tensor elements in the second laboratory frame, for the A_g irreducible representation

$$\alpha_{XX}^{(2)} = a \cos^2 \xi + (b \cos^2 \omega + c \sin^2 \omega) \sin^2 \xi + d \sin \omega \sin (2\xi)$$

$$\alpha_{XY}^{(2)} = (a - b \cos^2 \omega - c \sin^2 \omega) \sin \xi \cos \xi - d \sin \omega \cos (2\xi) = \alpha_{XY}^{(2)}$$

$$\alpha_{YY}^{(2)} = a \sin^2 \xi + (b \cos^2 \omega + c \sin^2 \omega) \cos^2 \xi - d \sin \omega \sin (2\xi)$$

For the B_g irreducible representation the tensor elements are

$$\alpha_{XX}^{(2)} = -e \cos \omega \sin (2\xi) - f \sin (2\omega) \sin^2 \xi$$

$$\alpha_{XY}^{(2)} = e \cos \omega \cos (2\xi) + f \sin \omega \cos \omega \sin (2\xi) = \alpha_{XY}^{(2)}$$

$$\alpha_{YY}^{(2)} = e \cos \omega \sin (2\xi) - f \sin (2\omega) \cos^2 \xi$$

The A_g and B_g vibrations of the NAGA crystal are essentially degenerate. The measured Raman intensity for each band is the sum of contributions from the A_g and B_g tensors. We can express the measured intensities in the lab(1) and the lab(2) frame as

functions of the Raman tensors elements of the A_g and B_g irreducible representations in the orthogonal crystallographic coordinate system by

$$I_{XX}(1) = a^2 \quad (\text{A8a})$$

$$I_{XY}(1) = d^2 \sin^2 \omega + e^2 \cos^2 \omega \quad (\text{A8b})$$

$$I_{YY}(1) = (b \cos^2 \omega + c \sin^2 \omega)^2 + f^2 \sin^2 (2\omega) \quad (\text{A8c})$$

$$I_{XX}(2) = [a \cos^2 \xi + (b \cos^2 \omega + c \sin^2 \omega) \sin^2 \xi + d \sin \omega \sin (2\xi)]^2 + [e \cos \omega \sin (2\xi) + f \sin (2\omega) \sin^2 \xi]^2 \quad (\text{A8d})$$

$$I_{XY}(2) = [(a - b \cos^2 \omega - c \sin^2 \omega) \sin \xi \cos \xi - d \sin \omega \cos (2\xi)]^2 + [e \cos \omega \cos (2\xi) + f \sin \omega \cos \omega \sin (2\xi)]^2 \quad (\text{A8e})$$

$$I_{YY}(2) = [a \sin^2 \xi + (b \cos^2 \omega + c \sin^2 \omega) \cos^2 \xi - d \sin \omega \sin (2\xi)]^2 + [e \cos \omega \sin (2\xi) - f \sin (2\omega) \cos^2 \xi]^2 \quad (\text{A8f})$$